Environ. Sci. Technol. **2007**, *41,* 6234−6239

Synergetic Effect of Bi_2WO_6 Photocatalyst with C_{60} and Enhanced Photoactivity under Visible Irradiation

SHENGBAO ZHU,[†] TONGGUANG XU,[†] HONGBO FU,[‡] JINCAI ZHAO,[§] AND YONGFA ZHU*,[†]

Department of Chemistry, Tsinghua University, Beijing, 100084, People's Republic of China, Department of Environmental Science and Engineering, Fudan University, Shanghai, 200433, People's Republic of China, Institute of Chemistry, Chinese Academy of Sciences, Beijing, 100080, People's Republic of China

Fullerene (C_{60})-modified Bi_2WO_6 photocatalyst is prepared by a simple absorbing process. The as-prepared samples show the high efficiency for the degradation of nonbiodegradable azodyes methylene blue (MB) and rhodamine B (RhB) under visible light ($\lambda > 420$ nm) and simulated solar light ($\lambda > 290$ nm). After being modified by C_{60}, the photocatalytic activities of Bi_2WO_6 samples increase about 5.0 and 1.5 times for the degradation of MB and RhB under visible light irradiation, whereas 4.6 and 2.1 times under xenon lamp irradiation, respectively. The enhanced photocatalytic activity for C_{60}-modified Bi_2WO_6 comes from the high migration efficiency of photoinduced electrons on the interface of C_{60} and Bi_2WO_6 which is produced by the interaction of Bi_2WO_6 and C_{60} with the conjugative π-system. The optimum synergetic effect is found at a weight ratio of 1.25 wt % (C_{60}/Bi_2WO_6). The photocatalytic reaction process of C_{60}-modified Bi_2WO_6 is mainly governed by direct holes and $O_2^{\bullet-}$ oxidation.

Introduction

Dye pollutants have been a major source of environmental pollution because of their resistance to biodegradation (*1*). Many conventional methods such as flocculation, reverse osmosis, and activated carbon adsorption have been used to deal with wastewaters containing dyes (*2*). However, many drawbacks still exist in these methods because of the increasing number of refractory materials in wastewater effluents and difficulties in the complete removal of color and expensiveness. Recent researches show that heterogeneous photocatalytic oxidation technologies are promising methods (*3*−*5*). Up to date, the majority of research on photocatalytic oxidation technologies is focused on dye/TiO_2 system (*6*−*8*). However, photoefficiency of the system and mineralization degree of dye is limited because of the slower interfacial electron transfer. Therefore, it is urgent to develop highly efficient visible-light induced photocatalysts for dye photodegradation.

* Corresponding author phone: +86-10-62783586; fax: +86-10-62787601; e-mail: zhuyf@mail.tsinghua.edu.cn.
[†] Tsinghua University.
[‡] Fudan University.
[§] Chinese Academy of Sciences.

Recent results reveal that Bi_2WO_6 photocatalyst can decompose water under visible light irradiation (*9*, *10*). Furthermore, nanosized Bi_2WO_6 performs as an excellent visible-light-driven photocatalyst for the destruction of dye pollutants with a high degree of mineralization (*11*, *12*). Fullerenes with the delocalized conjugated structures have gained extensive attentions for the interesting properties. One of the most remarkable properties in electron-transfer processes is that it can efficiently arouse a rapid photoinduced charge separation and a relatively slow charge recombination (*13*). Many works have focused on the photochemical solar cells by the combination of C_{60} and nanoparticles, which can greatly increase the photoconversion of solar energy (*14*, *15*). In general, the photocatalytic activity of the photocatalyst can be promoted by increasing the separation efficiency of photoinduced electron−hole pairs. Thus, the combination of photocatalysts and C_{60} may be an ideal system to achieve an enhanced charge separation by photoinduced electron transfer. Concerning the high photocatalytic activity of nanosized Bi_2WO_6, it is expected that the visible photoactivity of Bi_2WO_6 for degradation of dye can be enhanced via synergetic effect of C_{60} and Bi_2WO_6. In this work, C_{60}-modified Bi_2WO_6 photocatalyst is obtained by chemically adsorbing C_{60} on the surface of Bi_2WO_6. The photodegradation results of dyes over C_{60}-modified Bi_2WO_6 under visible-light irradiation and solar (simulated by xenon lamp) show that the photocatalytic activity can be significantly enhanced. It is postulated that the enhanced photoactivity of C_{60}-modified Bi_2WO_6 catalyst results from high migration efficiency of photoinduced electron−hole pairs.

Experimental Section

Preparation of Photocatalysts. Bi_2WO_6 was synthesized by the hydrothermal method according to ref *11*: the starting materials of Na_2WO_4 and $Bi(NO_3)_3$ were mixed together with the molar ratio of 1:2, deionized water (100 mL) was added, then white precipitates appeared immediately, and the mixed solution was ultrasonicated for 10 min to promote the precipitate reaction. The collected precipitate after washing several times was added into a 50 mL Teflon-lined autoclave and filled with deionized water up to 80% of the total volume. The autoclave was maintained at 180 °C for 20 h.

C_{60}-modified Bi_2WO_6 sample was prepared as follows: an appropriate amount of C_{60} was added into toluene and sonicated for 30 min to make C_{60} totally disperse. The as-prepared Bi_2WO_6 powder(1 g) was added into the above solution and stirred for 24 h. The solvent was evaporated at 80 °C for 10 h and opaque powder was obtained after drying. C_{60}-modified Bi_2WO_6 samples with other different mass ratio from 0.65 to 3.00% were prepared by following a similar procedure.

To investigate the transition of photogenerated electrons before and after C_{60} modification, Bi_2WO_6 film was prepared as follows: 0.02 mol Diethylenetriaminepentaacetic acid (H_5-DTPA) and 7.5 mL concentrated ammonia water (ca.13.0 mol·L^{-1}) were added in hot distilled water (200 mL). 0.005 mol Bi_2O_3 and 0.005 mol $5(NH_4)_2O{\cdot}12WO_3{\cdot}5H_2O$ powders were added afterward. The mixture was stirred and heated to promote the dissolution and reaction. After being slowly vaporized at 80 °C, transparent glass-like material was obtained. The as-prepared glass-like material was ground and redissolved in water to get the colorless transparent precursor solution with a concentration of 15 wt %. ITO (Indium Tin Oxide) glass substrates (3 cm × 2 cm) with a sheet resistance of 15 Ω were dipped into the complex precursor for 2 min and then were pulled out with a velocity

10.1021/es070953y CCC: $37.00
Published on Web 08/08/2007

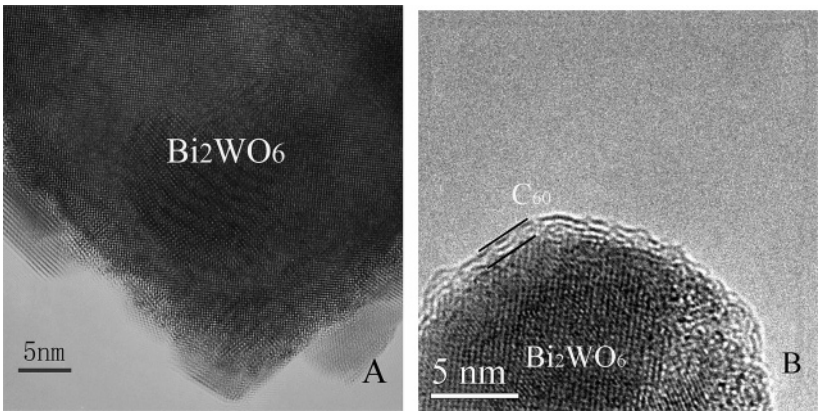

FIGURE 1. HRTEM images of (A) Bi_2WO_6 and (B) C_{60}-modified Bi_2WO_6 sample.

of 3 cm·min^{-1}. After being dried, the sample was heated to 450 °C and calcined for 4 h in air flow. Bi_2WO_6 film was dipped in a certain amount of C_{60} toluene solution for 20 h. The ITO glass covered with thin Bi_2WO_6 film and C_{60} were used as photoanode and named ITO/Bi_2WO_6 and ITO/Bi_2WO_6/C_{60}, respectively.

Characterization. HRTEM (high-resolution transmission electron microscopy) images were obtained by JEM 2010F field emission transmission electron microscope with an accelerating voltage of 200 kV. UV−visible absorption spectra of the samples were recorded on a UV−vis spectrophotometer (Hitachi UV-3100) with an integrated sphere attachment in the range of 200−800 nm. $BaSO_4$ was used as the reflectance standard. The Brunauer−Emmett−Teller (BET) surface area measurements were performed by a Micromeritics (ASAP 2010 V5.02H) surface area analyzer. The nitrogen adsorption and desorption isotherms were measured at 77 K after degassing the samples on a Sorptomatic 1900 Carlo Erba Instrument.

Photocatalytic and Photoelectrochemical Performance. The photocatalytic activities were evaluated for the degradation of RhB and MB solution under visible light and simulated solar irradiation. A 500 W xenon lamp (λ > 290 nm Institute of Electric Light Source, Beijing) with a 420 nm cutoff filter was used as light resource, and the average light intensity was 30 mW·cm^{-2}. 100 mg of the C_{60}-modified Bi_2WO_6 photocatalyst was dispersed in 1×10^{-5} mol·L^{-1} RhB or MB solution (100 mL). Prior to the irradiation, the suspension was magnetically stirred in the dark for 30 min to reach an absorption−desorption equilibrium. At a given time interval, 3 mL aliquots were sampled and centrifuged to remove the particles. The degradation of RhB and MB were monitored by a Hitachi U-3010 UV−vis spectrophotometer. The concentration of RhB and reaction intermediates were measured by HPLC (high performance liquid chromatography) using an Intersil ODS-3C-18 inversed-phase column. All samples were detected by a UV−vis detector at 505 nm. The solution gradient was regulated by water and methanol (from 60 to 90% methanol over 25 min) with a flow rate of 1 mL·min^{-1}.

Photoelectrochemical measurements were carried out in a conventional three-electrode, single-compartment glass cell, fitted with a synthesized quartz window, using a potentiostat. The quartz electrolytic cell was filled with 0.5 M Na_2SO_4 and 10^{-5} M MB solution (100 mL). The ITO/Bi_2WO_6/C_{60} or ITO/Bi_2WO_6 electrodes served as the working electrode. The counter and the reference electrodes were platinum black wire and saturated calomel electrode (SCE), respectively. A 30 W germicidal lamp was used as the excitation light source. The incident light was irradiated onto electrodes from the front face through the quartz window and the electrolyte unless noted otherwise. The irradiated light intensity was 1 mW·cm^{-2}. The photoelectrochemical experiment was measured on electrochemical system (CHI-660B, China).

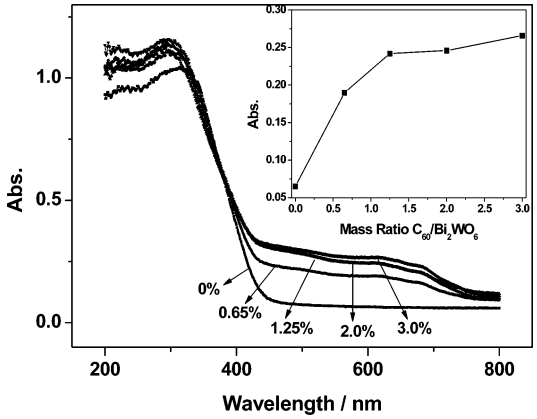

FIGURE 2. UV−vis DR spectra of Bi_2WO_6 and C_{60}/Bi_2WO_6 samples with various mass ratios. Inset: changes of absorbance (600 nm) as a function of mass ratio C_{60}/ Bi_2WO_6.

Results and Discussion

Structure and Optical Properties of C_{60}-modifed Bi_2WO_6 Photocatalyst. Figure 1 shows the morphologies and lattice structure of Bi_2WO_6 and C_{60}-modified Bi_2WO_6. It was found that the lattice structure of Bi_2WO_6 was clear from the center to the boundary (Figure 1A), and there was no change of lattice structure of Bi_2WO_6 after C_{60} adsorbed on the surface. However, the outer boundary of Bi_2WO_6 modified by C_{60} was distinctly different. A coverture layer with noncrystal structure surrounded the surface of Bi_2WO_6 nanosheet. The thickness of the coverture layer was estimated to be about 1 nm, which was close to the diameter of C_{60} molecular. Therefore, it can be estimated that the outer layer was C_{60}, which dispersed on the surface of Bi_2WO_6 with a monolayer structure. XRD (X-ray diffraction) patterns of Bi_2WO_6 sample showed no change when Bi_2WO_6 was modified by C_{60}, indicating the absorption of C_{60} did not influence the lattice structure of Bi_2WO_6. No XRD diffraction peaks assigned to C_{60} was observed because the C_{60} layer was too thin.

The diffuse-reflection spectra (DRS) of Bi_2WO_6 and C_{60}-modified Bi_2WO_6 with different C_{60}/Bi_2WO_6 mass ratios are depicted in Figure 2. Bi_2WO_6 sample showed an absorption edge around 470 nm, which could be responsible for the visible-light induced photocatalytic activity. With the loading of C_{60}, the C_{60}/Bi_2WO_6 displayed the same absorption edge as Bi_2WO_6. However, the samples exhibited a greater light attenuation throughout the visible wavelengths consistent with the grayed color of the catalyst. It also could be found

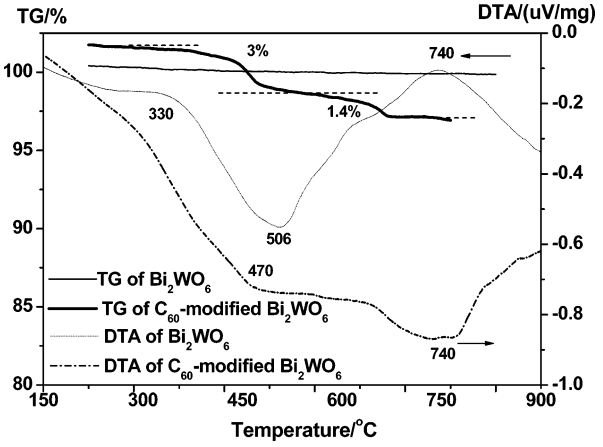

FIGURE 3. TG and DTA curves of Bi_2WO_6 and C_{60}-modified Bi_2WO_6 in the presence of N_2.

that the absorption intensity of the prepared samples changed with the increasing of C_{60}/Bi_2WO_6 weight ratio. The absorption intensity increased rapidly with C_{60}/Bi_2WO_6 from 0.65 to 1.25%, but the increment was small from 1.25 to 3.0%. It was interesting that the absorbance of samples at 600 nm changed with a function of mass ratio of C_{60}/ Bi_2WO_6 (inset of Figure 2). Considering the diameter of C_{60} (0.71 nm) and the BET surface area of Bi_2WO_6 (8.68 m^2 g^{-1}), it can be estimated that the weight ratio about 2.0% with a nearly compact C_{60} monolayer coverage on Bi_2WO_6. The actual concentration of C_{60} absorbed on the surface of Bi_2WO_6 could be even less than 2.0% because C_{60} can only occupy the active absorption site. Based on the absorption spectra, the intensity remained almost unchanged when the ratio of C_{60}/ Bi_2WO_6 increased from 1.25 to 2.0%, indicating that C_{60} may aggregate to form cluster on the surface of Bi_2WO_6 nanosheet when the weight ratio of C_{60}/Bi_2WO_6 was above 2.0%.

The absorption states of C_{60} on the surface of Bi_2WO_6 sample can be revealed by the thermogravimetry and differential thermal analyses (TG-DTA). TG-DTA curves of Bi_2WO_6 sample before and after modified by C_{60} are shown in Figure 3. As for Bi_2WO_6, there was no weight loss can be discerned from TG curve, but the endothermic and exothermic peaks appeared on DTA curve. The endothermic peak at 330 °C might be attributed to the loss of water and another endothermic peak at 740 °C was attributed to the phase transform of Bi_2WO_6 (*16*, *17*). The exothermic peak at 506 °C appeared and could be caused by the decomposition of absorbed solvent. Two weight loss regions resulting from C_{60}-modified Bi_2WO_6 sample appeared in TG curve. The total weight loss was about 4.4% in two regions. The first weight loss of 3% occurring from 300 to 500 °C could be attributed to the desorption of solvent. The second weight loss was about 1.4%, which was nearly consistent to the amount of C_{60} modified on the surface of Bi_2WO_6 (1.25%). The exothermic peak at 450 °C was also related to the physical desorption of C_{60}. Compared with Bi_2WO_6, a wide exothermic peak at 740 °C was related to the chemical desorption of C_{60}. It should be noted that the endothermic peak of phase transformation for the Bi_2WO_6 modified by C_{60} may shift to 900 °C, demonstrating the inhibition of the phase transformation by C_{60} monolayer.

The pore size distributions of C_{60}/Bi_2WO_6 sample were measured by BJH desorption isotherms. Results showed that the pore size of Bi_2WO_6 modified by C_{60} had a similar distribution as Bi_2WO_6, which was about 3.45 nm (see Supporting Information Figure S1). The pore volume and the pore diameter decreased slightly after C_{60} modification. The decrease of the pore volume and the pore size may be ascribed to C_{60} molecule occupying the adsorption site which was partly in the pores (*18*). These N_2 (Figure S1, inset) isotherms exhibited a hysteresis loop, which could be attributed to the total contribution of both interparticle and intraparticle pores. There was no appreciable change in the surface area (BET surface area of Bi_2WO_6 and C_{60}-modified Bi_2WO_6 was 8.68 $m^2 \cdot g^{-1}$ and 8.36 $m^2 \cdot g^{-1}$, respectively). The above results also implied that the modification of C_{60} did not obviously change the pore structure of Bi_2WO_6. Based on the results of HRTEM, DR spectra, pore size distribution, and TG-DTA measurement, it could be concluded that C_{60} molecule adsorbed on the surface of Bi_2WO_6 forming a monomolecular layer and an intimate contact existed between C_{60} and Bi_2WO_6 phase.

Photocatalytic Activities. The photocatalytic activity of the as-prepared sample was first evaluated by the degradation of MB in aqueous solution. Figure 4A shows the photocatalytic degradation curve of normalized MB as a function of time. The first-order linear relationship was revealed by the plots of $\ln(C/C_0)$ vs irradiation time. The blank test confirmed that MB was not degraded in the dark and only slightly degraded under visible light in the absence of catalysts, indicating that the photolysis and adsorption action of catalysts can be ignored. Only 25% MB can be photodegraded by Bi_2WO_6 under visible light in 2 h. All the modified Bi_2WO_6 samples exhibited higher photocatalytic activities than pure Bi_2WO_6. The sample with 1.25% C_{60} showed the highest activity, 80% of MB can be photodegraded under the same condition. Results showed that the loading amount of C_{60} had a great influence on the photocatalytic activity of the as-prepared photocatalyst. The influence of C_{60} loading amounts upon the photodegradation rate of MB is shown in Figure 4A, the apparent reaction rate constant k was 0.0037, 0.0099, 0.0069, 0.0033, and 0.0020 min^{-1}, respectively, for C_{60}/Bi_2WO_6 ratio of 0.65%, 1.25%, 2.0%, 3.0%, and Bi_2WO_6 samples. When the loading amount was below 1.25%, the photocatalytic activities increased with the increase of loading amount of C_{60}. The

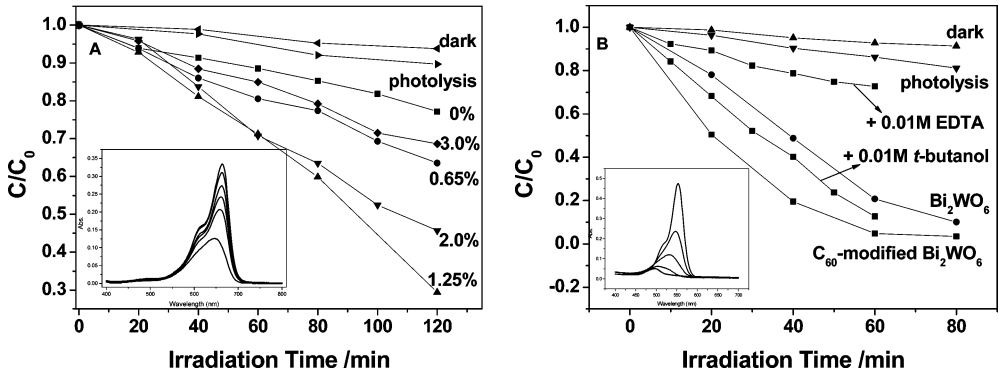

FIGURE 4. Photocatalytic degradation of (A) MB and (B) RhB by C_{60}-modified Bi_2WO_6 and Bi_2WO_6 under visible light irradiation ($\lambda > 420$ nm). Inset: Absorption changes of (A) MB and (B) RhB solution under photocatalytic process.

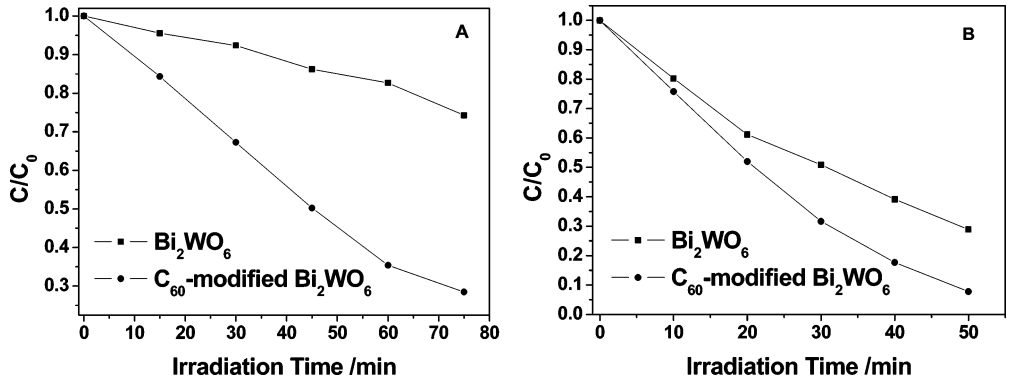

FIGURE 5. Photocatalytic degradation of (A) MB and (B) RhB over 1.25% C_{60}-modified Bi_2WO_6 and Bi_2WO_6 under Xenon lamp irradiation (λ > 290 nm, simulated solar irradiation).

degradation ratio of MB increased from 36 to 71% with the mass ratio C_{60}/Bi_2WO_6 from 0.65 to 1.25% after irradiation for 120 min. However, when the loading amount of C_{60} exceeded 1.25%, the photocatalytic activities of samples decreased as the amount of C_{60} increased. The optimal loading amount of C_{60} on Bi_2WO_6 for increasing the photocatalytic activity was 1.25%. As mentioned in the result of DRS, C_{60} tended to aggregate on the surface of Bi_2WO_6 when the mass ratio of C_{60} above 1.25%, which resulted in the slower transmission of the photoinduced electrons. 1.25% C_{60} and Bi_2WO_6 mechanical mixture as a reference was prepared by merely stirring. Its photocatalytic activity was similar to that of Bi_2WO_6 and much lower compared with 1.25% C_{60}-modified Bi_2WO_6 catalyst. The photocatalytic activity of Bi_2WO_6 modified by C_{60} was enhanced by about 4 times compared with that of Bi_2WO_6 sample. This result implied that the interaction between C_{60} and Bi_2WO_6 photocatalyst took an important role in the enhancement of photoactivity. The photocatalytic decomposition of RhB by 1.25% C_{60}-modified Bi_2WO_6 and Bi_2WO_6 samples under visible light irradiation was also carried out (Figure 4B). C_{60}-modified Bi_2WO_6 sample showed much higher photocatalytic activity for the decomposition of RhB than Bi_2WO_6. The apparent reaction rate constant k was 0.0454 and 0.0296 min^{-1} for C_{60}-modified Bi_2WO_6 and Bi_2WO_6 samples, respectively. Therefore, it was a novel way to enhance the photocatalytic activity of Bi_2WO_6 by modifying with C_{60}.

The temporal evolution of the spectral changes taking place during the photodegradation of RhB over Bi_2WO_6 were displayed (Figure 4B, inset). During the degradation, the absorption maximum of the degraded solution with irradiation time exhibited hypsochromic shifted to some extent with the cleavage of the conjugated structure (*12*), while, the MB decomposition under visible irradiation mainly occurred via the destruction of the conjugated structure (Figure 4A, inset) (*19*). The photodecomposition process of RhB under visible-light irradiation was demonstrated by HPLC. The typical HPLC chromatograms in the presence of Bi_2WO_6 and C_{60}-modified Bi_2WO_6 were recorded by UV−visible detector. After 70 min, the concentration of RhB in C_{60}-modified Bi_2WO_6 system (see Supporting Information Figure S2B) was much lower than that in Bi_2WO_6 system (see Supporting Information Figure S2A). The evidence further proved that the reaction rate of Bi_2WO_6 modified by $C_{60}$was faster. At the same time, no new intermediates or products formed, indicating the photocatalytic decomposition process for pollutants was similar with Bi_2WO_6 even after being modified by C_{60}.

The photocatalytic performance of Bi_2WO_6 modified by C_{60} under simulated solar irradiation was also studied. In this work, xenon lamp was used to simulate the solar irradiation. The photocatalytic performances of C_{60}-modified Bi_2WO_6 sample are shown in Figure 5. The apparent reaction rate constants k were 0.0175, 0.0038 min^{-1} of C_{60}-modified Bi_2WO_6 and Bi_2WO_6 for the decomposition of MB, and 0.0504, 0.0244 min^{-1} for the decomposition of RhB. C_{60}-modified Bi_2WO_6 sample can effectively decompose dyes under simulated solar condition, which was similar to the result under visible light irradiation. It was well-known that the photocatalytic activity was governed by various factors such as surface area, phase structure, interfacial charge transfer, and separation efficiency of photoinduced electrons and holes (*20*). Results showed that the surface area and phase structure of Bi_2WO_6 almost remained the same before and after being modified by C_{60}. It could be concluded that the difference of photocatalytic activity was not determined by the factor of surface area and phase structure. Therefore, the enhancement of photocatalytic activity may be attributed to the high separation efficiency of electron and hole pairs.

Interestingly, it is found that the enhancement degree of photocatalytic activity for the photodegradation of MB and RhB by 1.25% C_{60}-modified Bi_2WO_6 under simulated solar irradiation is different. The photocatalytic activity increased much more for the degradation of MB than for the degradation of RhB. The difference in enhancement of photocatalytic activity may result from the difference in photocatalytic reaction mechanism. For the photodegradation of RhB, the photosensitization process mainly governed photocatalytic reaction process. RhB molecules absorbed the incident photon flux, and the photogenerated electrons transferred to the excited-state of the dye (*21*). Then the photoelectrons of the excited-state were immediately injected into the conduction band (W 5d level) of Bi_2WO_6 (*12*). Finally, the RhB absorbed on the surface of Bi_2WO_6 react with the active species generated on the surface. However, the electron cannot migrate from RhB to Bi_2WO_6 after being modified by monomolecular layer C_{60} for the incompatibility of energy level. The photosensitization process for RhB was inhibited; therefore, the photocatalytic activity was decreased. However, the existence of C_{60} can greatly promote the transfer of the photoinduced electron which resulted in the enhancement of the separation efficiency for electron and hole pairs. The above two competitive effects finally caused the photodecolorization activity for RhB to only be improved by 1.5 times. For the photocatalytic degradation of MB, direct photocatalytic reaction was the main process and no inhibition effect of photosensitization process could occur in the system (*22*). Therefore, the promotion of electron transfer by modified C_{60} caused the drastic enhancement of photocatalytic activity (4.3 times). The photocatalytic reaction process was also studied by adding a scavenger of radicals and capture of holes. As shown in Figure 4, the addition of a scavenger of hydroxyl radicals (tert-butanol) only caused small change in the degradation rate of RhB, indicating that the free hydroxyl radicals was not the main active oxygen species in the photochemical process. On the contrary, the photocatalytic

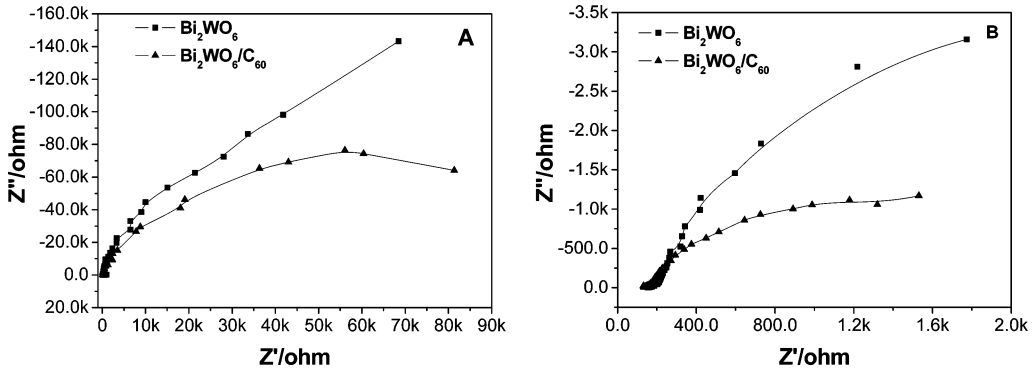

FIGURE 6. EIS Nynquist plots of ITO/Bi_2WO_6/C_{60} electrode and ITO/Bi_2WO_6 electrode under (A) visible light irradiation (λ > 420 nm) and (B) xenon lamp irradiation.

SCHEME 1. Possible Pathway of the Photoelectron Transfer Excited by Visible Light Irradiation Including Photocatalytic Process for C_{60}-modified Bi_2WO_6

activity of Bi_2WO_6 after being modified by C_{60} could be greatly inhibited by the addition of capture for holes (EDTA-Na). ESR (electron spin resonance) spin-trap technique (with DMPO) was employed to monitor the reactive oxygen species generated during the irradiation of the present system (see Supporting Information Figure S3). No DMPO-•OH signals appeared when the RhB/Bi_2WO_6 and the RhB/C_{60}-modified Bi_2WO_6 suspension were irradiated by a Quanta-Ray Nd: YAG pulsed laser system (λ = 532 nm, 10 Hz) (Figure S3A). But the •OOH/$O_2^{\bullet-}$ adducts were observed for the RhB/C_{60}-modified Bi_2WO_6 system under this pulsed laser irradiation (Figure S3B). The radical scavenger technologies and kinetic studies by using ESR suggested that •OH racial oxidation reaction was not the dominant photooxidant pathway. Direct hole transfers and $O_2^{\bullet-}$ oxidation reaction mainly govern the photocatalytic process. The enhancement of photocatalytic activity could be attributed to the higher separation efficiency of electron−hole pairs caused by the rapid photoinduced charge separation and the inhibition of recombination for electron−hole pairs of C_{60}, resulting in the increasing of number of holes participated in the photooxidation process and enhancing of photocatalytic activity.

Photocatalytic Mechanism. As discussed above, the C_{60}-modified Bi_2WO_6 photocatalyst showed a high photocatalytic activity under both visible and simulated solar irradiation. The reason should be closely attributed to the interaction between Bi_2WO_6 and C_{60} which increased the photogenerated electron mobility in Bi_2WO_6. In this work, C_{60} molecule was mainly covered on the surface of Bi_2WO_6. C_{60} acted as an electron shuttle that could effectively transfer the photoelectrons from conduction band of Bi_2WO_6 after being illuminated under visible light irradiation. The delocalized conjugated π structure of C_{60} made it easier to transfer the photoinduced electrons (*15*). Accordingly, the photogenerated electrons in the modified Bi_2WO_6 photocatalyst could easily migrate from the inner region to the surface to take part in the surface reaction. Based on the above discussion, the schematic of photocatalytic mechanism was shown in Scheme 1.

The effect of C_{60} modification on the recombination of e^-/h^+ produced by Bi_2WO_6 was also investigated. PL spectra were measured for Bi_2WO_6 nanoparticles and C_{60}-modified Bi_2WO_6 (see Supporting Information Figure S4). There were two peaks at about 486 and 461 nm at room temperature for the Bi_2WO_6 sample, which were attributed to the radiative recombination process of self-trapped excitions (*23*). The position of the emission peaks of Bi_2WO_6 after being modified with C_{60} on the surface remained almost unchanged, suggesting that the interaction between C_{60} and Bi_2WO_6 was chemical absorption. The PL peak intensity of C_{60}-modified Bi_2WO_6 sample was weaker than that of pure Bi_2WO_6. The great reduction of PL intensity indicated the decrease of radiative recombination process. Thus, the recombination of e^-/h^+ excited in Bi_2WO_6 under visible light could be inhibited by modifying with C_{60}. Furthermore, electrochemical impedance spectroscopy (EIS) was also used to investigate the photogenerated charge separations process on ITO/Bi_2WO_6 film and ITO/Bi_2WO_6/C_{60} film. Figure 6 shows EIS response of ITO/Bi_2WO_6 film sample and ITO/Bi_2WO_6/C_{60} film sample under visible light (λ > 420 nm) irradiation. The radius of the arc on the EIS Nynquist plot reflects the reaction rate occurring at the surface of electrode. The arc radius on EIS Nynquist plot of ITO/Bi_2WO_6/C_{60} film was smaller than that of ITO/Bi_2WO_6 film sample, which meant that an effective separation of photogenerated electron−hole pairs and fast interfacial charge transfer to the electron donor/electron acceptor occurred as suggested (*24*, *25*). Under simulated solar irradiation (λ > 290 nm), a similar result was obtained. The arc radius on EIS Nynquist plot of ITO/Bi_2WO_6/C_{60} film sample became smaller after being modified by C_{60} on the film of ITO/Bi_2WO_6. Hence, it could be concluded that there also existed an effective separation of the photogenerated electron−hole pair and a fast interfacial charge transfer to the electron donor/electron acceptor after Bi_2WO_6 film was modified by C_{60} under visible and simulated solar irradiation. Figure S5 shows the applied potential dependence of the photocurrent for ITO/Bi_2WO_6/C_{60} film and ITO/Bi_2WO_6 film (450 W Xe lamp; electrolyte, 0.1 M Na_2SO_4 solution). An obvious anodic photocurrent was obtained when anodic bias potential was present. No photocurrent can be found for ITO/Bi_2WO_6 film at V = 0.9 V in the dark. The photocurrent of ITO/Bi_2WO_6 increased to 1.41×10^{-4} A when illuminated by Xe lamp. It is interesting that the photocurrent of ITO/Bi_2WO_6/C_{60} film increased to 2.56×10^{-4} A, which increased about two times after being modified by C_{60}, suggesting the improvement of separation efficiency and inhibition of recombination of photoinduced electron−hole pairs. These photoelectric characteristics further proved that the combination of Bi_2WO_6 and electron acceptor (C_{60}) was an effective way to improve photocatalytic efficiency.

The stability of the photocatalyst was also studied. The DR spectra of C_{60}-modified Bi_2WO_6 changed very little after

UV irradiation for 10 days (see Supporting Information Figure S6), further confirming that the interaction between C_{60} and Bi_2WO_6 was strong and the modified Bi_2WO_6 photocatalyst was very stable under irradiation. The photocatalytic activity after irradiation was nearly the same as before, indicating that the C_{60}-modified Bi_2WO_6 photocatalyst is fairly stable under the studied conditions.

The storing and shuttling photoinduced electrons role of C_{60} in a photocatalytic process is realized by coating Bi_2WO_6 with monomolecular layer C_{60}. It is the electronic contact between semiconductor and C_{60} that lead to the efficient separation of electron−hole pairs to reduce electron−hole recombination, which exhibits high photocatalytic activity under visible light and simulated solar light irradiation. In conclusion, the modified photocatalyst is an interesting and promising photocatalytic material which has good potential for application to pollutants purification.

Acknowledgments

This work was partly supported by Chinese National Science Foundation (20433010 20673065) and SRFDP (2006003082).

Supporting Information Available

ESR experiment, Figures S1−S6. This material is available free of charge via the Internet at http://pubs.acs.org.

Literature Cited

(1) Raffainer, I. I.; Rudolf von Rohr, P. Promoted wet oxidation of the Azo dye orange II under mild conditions. *Ind. Eng. Chem. Res.* **2001**, *40*, 1083−1089.

(2) Herrera, F.; Lopez, A.; Mascolo, G.; Albrs, P.; Kiwi, J. Catalytic decomposition of the reactive dye Unibluea on hematite modeling of the reactive surface. *Water Res.* **2001**, *35*, 750−760.

(3) Liu, G. M.; Wu, T. X.; Zhao, J. C.; Hidaka, H.; Serpone, N. Photoassisted degradation of dye pollutants. 8. Irreversible degradation of alizarin red under visible light radiation in air-equilibrated aqueous TiO_2 dispersions. *Environ. Sci. Technol.* **1999**, *3*, 2081−2087.

(4) Wu, T. X.; Lin, T.; Zhao, J. C.; Hidaka, H.; Serpone, N. TiO_2-assisted photodegradation of dyes. 9. photooxidation of a squarylium cyanine dye in aqueous dispersions under visible light irradiation. *Environ. Sci. Technol.* **1999**, *33*, 1379−1387.

(5) Chen, C. C.; Zhao, W.; Li, J. Y.; Zhao, J. C.; Hidaka, H.; Serpone, N. Formation and identification of intermediates in the visible-light-assisted photodegradation of sulforhodamine-B dye in aqueous TiO_2 dispersion. *Environ. Sci. Technol.* **2002**, *36*, 3604−3611.

(6) Vinodgopal, K.; Wynkoop, D. E.; Kamat, P. V. Environmental photochemistry on semiconductor surfaces: photosensitized degradation of a textile Azo dye, acid Orange 7, on TiO_2 particles using visible light. *Environ. Sci. Technol.* **1996**, *30*, 1660−1666.

(7) Ehret, A.; Stuhl, L.; Spitler, M. T. Spectral sensitization of TiO_2 nanocrystalline electrodes with aggregated cyanine dyes. *J. Phys. Chem. B* **2001**, *105*, 9960−9965.

(8) Konstantinou, I. K.; Albanis, T. A. TiO_2-assisted photocatalytic degradation of azo dyes in aqueous solution: Kinetic and mechanistic investigations: a review. *Appl. Catal. B* **2004**, *49*, 1−14.

(9) Kudo, A.; Hijii, S. H_2 or O_2 evolution from aqueous solutions on layered oxide photocatalysts consisting of Bi^{3+} with $6s^2$ configuration and d^0 transition metal ions. *Chem. Lett.* **1999**, 1103−1104.

(10) Tang, J. W.; Zou, Z. G.; Ye, J. H. Photocatalytic decomposition of organic contaminants by Bi_2WO_6 under visible light irradiation. *Catal. Lett.* **2004**, *92*, 53−56.

(11) Zhang, C.; Zhu, Y. F. Synthesis of square Bi_2WO_6 nanoplates as high-activity visible-light-driven photocatalysts. *Chem. Mater.* **2005**, *17*, 3537−3545.

(12) Fu, H. B.; Pan, C. S.; Yao, W. Q.; Zhu, Y. F. Visible-light-induced degradation of rhodamine B by nanosized Bi_2WO_6. *J. Phys. Chem. B* **2005**, *109*, 22432−22439; Fu, H. B.; Zhang, L. W.; Yao, W. Q.; Zhu, Y. F. Photocatalytic properties of nanosized Bi_2WO_6 catalysts synthesized via a hydrothermal process. *Appl. Catal., B* **2006**, *66*, 100−110.

(13) Yu, G.; Gao, J.; Hummelen, J. C.; Wudl, F.; Heeger, A. J. Polymer photovoltaic cells: Enhanced efficiencies via a network of internal donor-acceptor heterojunctions. *Science* **1995**, *270*, 1789−1791.

(14) Kamat, P. V.; Gevaert, M.; Vinodgopal, K. Photochemistry on semiconductor surfaces. Visible light induced oxidation of C_{60} on TiO_2 nanoparticles. *J. Phys. Chem. B.* **1997**, *101*, 4422−4427.

(15) Hasobe, T.; Imahori, H.; Fukuzumi, S.; Kamat, P. V. Light energy conversion using mixed molecular nanoclusters. Porphyrin and C_{60} cluster films for efficient photocurrent generation. *J. Phys. Chem. B* **2003**, *107*, 12105−12112.

(16) Yanovskii, V. K.; Voronkova, V. I. Polymorphism and properties of Bi_2WO_6 and Bi_2MoO_6. *Phys. Status Solidi A* **1986**, *93*, 57−66.

(17) Zhang, S. C.; Zhang, C.; Man, Y.; Zhu, Y. F. Visible-light-driven photocatalyst of Bi_2WO_6 nanoparticles prepared via amorphous complex precursor and photocatalytic properties. *J. Solid. State. Chem.* **2006**, *179*, 62−69.

(18) Shanmugam, S.; Gabashvili, A.; Jacob, D. S.; Yu, J. C.; Gedanken, A. Synthesis and characterization of TiO_2@C core-Shell composite nanoparticles and evaluation of their photocatalytic activities. *Chem. Mater.* **2006**, *18*, 2275−2282.

(19) Chen, C. C.; Li, X.; Ma, W. H.; Zhao, J. C.; Hidaka, H.; Serpone, N. Effect of transition metal ions on the TiO_2-assisted photodegradation of dyes under visible irradiation: A probe for the interfacial electron transfer process and reaction mechanism. *J. Phys. Chem. B* **2002**, *106*, 318−324.

(20) Linsebigler, A. L.; Lu, G.; Yates, J. T., Jr. Photocatalysis on TiO_2 surfaces: principles, mechanisms, and selected results. *Chem. Rev.* **1995**, *95*, 735−758.

(21) Yang, J.; Chen, C. C.; Ji, H.; Ma, W. H.; Zhao, J. C. Mechanism of TiO_2-assisted photocatalytic degradation of dyes under visible irradiation: photoelectrocatalytic study by TiO_2-film electrodes. *J. Phys. Chem. B* **2005**, *109*, 21900−21907.

(22) Park, H.; Choi, W. Photocatalytic reactivities of Nafion-coated TiO_2 for the degradation of charged organic compounds under UV or visible Light. *J. Phys. Chem. B.* **2005**, *109*, 11667−11674.

(23) Yu, S. H.; Liu, B.; Mo, M. S.; Huang, J. H.; Liu, X. M.; Qian, Y. T. General synthesis of single-crystal nanorods/nanowires: a facile, low-temperature solution approach. *Adv. Funct. Mater.* **2003**, *13*, 639−647.

(24) Leng, W. H.; Zhang, Z.; Zhang, J. Q.; Cao, C. N. Investigation of the kinetics of a TiO_2 photoelectrocatalytic reaction involving charge transfer and recombination through surface states by electrochemical impedance spectroscopy. *J. Phys. Chem. B* **2005**, *109*, 15008−15023.

(25) Liu, H.; Cheng, S. A.; Wu, M.; Wu, H. J.; Zhang, J. Q.; Li, W. Z.; Cao, C. N. Photoelectrocatalytic degradation of sulfosalicylic acid and its electrochemical impedance spectroscopy investigation. *J. Phys. Chem. A* **2000**, *104*, 7016−7020.

Received for review April 23, 2007. Revised manuscript received June 24, 2007. Accepted July 2, 2007.

ES070953Y